ACS APPLIED MATERIALS & INTERFACES

Research Article

www.acsami.org

Polyol-Assisted Vermiculite Dispersion in Polyurethane Nanocomposites

Yong Tae Park,[†] Yuqiang Qian,[‡] Chris I. Lindsay,[§] Conny Nijs,[§] Rafael E. Camargo,[∥] Andreas Stein,*[,‡] and Christopher W. Macosko*[,†]

[†]Department of Chemical Engineering and Materials Science and [‡]Department of Chemistry, University of Minnesota, Minneapolis, Minnesota 55455, United States

[§]Huntsman Polyurethanes, Everslaan 45, 3078 Everberg, Belgium

[∥]Huntsman Polyurethanes, 8600 Gosling Rd., The Woodlands, Texas 77381, United States

Supporting Information

ABSTRACT: The largest use of polyurethane (PU) is as closed cell rigid foams for thermal insulation. One problem is loss of blowing gases, which leads to slow increase in thermal conductivity. PU composites with plate-like nanofillers create a diffusion barrier, reducing gas transport and slowing insulation aging. In this research, a new in situ intercalative polymerization is described to disperse vermiculite (VMT) in PU. When VMT was modified by cation exchange with long-chain quaternary ammonium, the dispersion in methylene diphenyl diisocyanate (MDI) was significantly improved. Dispersion of clay in MDI was further improved by combining high intensity dispersive mixing with a polyol-clay preblend (master-batch). The VMT dispersibility was characterized using rheology, microscopy, and X-ray scattering/diffraction. With the method of polyol-assisted VMT dispersion, electron microscopy revealed extensive intercalation and exfoliation of clay particles. In contrast, simple mixing of organoclay in MDI resulted in macroscopic localization and poor distribution of clay particles in PU. The final nanocomposites prepared by the master-batch method showed enhancement of mechanical properties (85% increase in elastic modulus) and reduction in permeability to CO_2, as much as 40%, at a low clay concentration of 3.3 wt %.

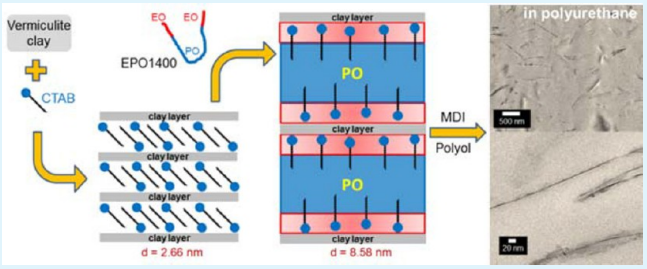

KEYWORDS: *vermiculite, polyurethane, organoclay, polymer−clay nanocomposite, gas barrier*

1. INTRODUCTION

Polyurethane (PU) is used for a variety of applications, from foams to elastomers and films, whose properties depend on the type and functionality of the polyols and isocyanates.[1,2] Twenty-three percent of all PU production is used for rigid foams, primarily in thermal insulation.[3] PU rigid foams have excellent qualities, such as a higher strength-to-weight ratio and better thermal insulation than thermoplastic foams or other common insulation materials. However, PU foams are subject to thermal aging where thermal conductivity of the materials steadily increases over time, since CO_2 with low thermal conductivity slowly diffuses out from the cells and is replaced by N_2 and O_2, which present a higher thermal conductivity.[3,4] One way to slow down this thermal aging is to reinforce foams with diffusion-barrier particles. In particular, layered clays are excellent candidates for reducing diffusion in PU.[5−7] Clays have also been used to improve properties of elastomeric and rigid PUs.[5−13] The enhancement of mechanical properties, such as strength, modulus, and fracture toughness, and the reduction in thermal conductivity and gas permeation have been investigated.[5,6,8−13]

Most previous studies of polymer−clay nanocomposites have focused on montmorillonite (MMT) clay.[6,8−12] Vermiculite (VMT), however, is an economical natural clay that is globally produced at 500k tons per year.[14,15] It is mainly used in high-temperature, refractory, and acoustic insulation and has seen little application with PU or other polymers because of difficult dispersibility. Only a few studies of polymer-VMT nanocomposites have been reported.[5,13,16−18] Like MMT, VMT forms sheet-like crystals with high-aspect-ratio which are potentially suitable as diffusion barriers after exfoliation. Compared with MMT, the relatively high charge density of VMT sheets makes them harder to exfoliate. However, incorporation of cationic organic modifiers increases interlayer spacing.[19] Organic modification with quaternary alkyl ammonium ions helps to expand the interlayers of VMT clay.[5,20] The dispersions of nano-VMT clays in PU components and their effect on the mechanical properties and barrier properties of elastomeric PU were also characterized.[5,20] However, VMT has not yet been exfoliated in PU rigid systems.

In this study, the goal was the improvement of gas barrier properties of rigid PU by organically modified VMT clay to

Received: December 25, 2012
Accepted: March 18, 2013
Published: March 18, 2013

reduce the thermal aging. Organically modified VMT was dispersed in polymeric methylene diphenyl diisocyanate (MDI), and then PU-VMT nanocomposites were fabricated by bulk in situ polymerization with polyether-based polyols. A series of modifications made clay platelets better dispersible in PU. Dispersion and intercalation of the modified clay in polymeric MDI were characterized by rheology, X-ray scattering, and microscopy. Intercalation or exfoliation of organoclay in the PU matrix was characterized by transmission electron microscopy (TEM). Gas barrier properties can only be inferred indirectly on rigid foam via thermal aging which is also a time-consuming process. Thus, rigid PU nanocomposite films, not foams, were produced, and their thermal and mechanical properties and CO_2 permeation were measured.

2. EXPERIMENTAL SECTION

2.1. Materials. Natural VMT (Grade 3, thermally expanded) was purchased from Sigma-Aldrich and jet-milled by Hosokawa Micron, U.K. Jet-milled VMT has a particle size of less than 5 μm with an average of 3 μm (Supporting Information, Figure S1). Sodium chloride (VMR Inc.), ethanol (200 proof, Decon Laboratories Inc.), cetyltrimethylammonium bromide (CTAB, 99%, Sigma-Aldrich, Figure 1), polymeric MDI (Rubinate M, Huntsman Polyurethanes,

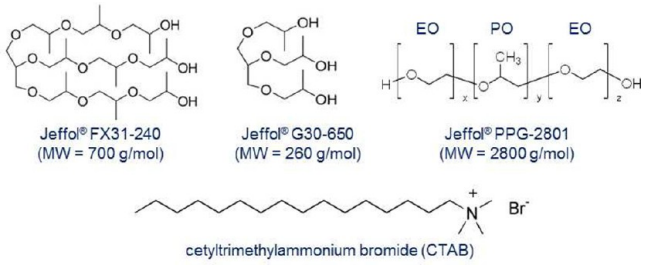

Figure 1. Chemical structures of three different polyols and the CTAB modifier.

functionality = 2.7, 31.2% NCO, equivalent weight = 135 g/mol), silicone defoamer (BYK-88, BYK-USA), and toluene (Sigma-Aldrich) were used as received. Three Huntsman Polyurethanes polyols (see Figure 1), Jeffol G30-650 (trifunctional, all propylene oxide (PO), glycerin initiated, M_n = 260 g/mol), Jeffol FX31-240 (trifunctional, all PO glycerin initiated, M_n = 700 g/mol), and Jeffol PPG-2801 (difunctional, ethylene oxide (EO) tipped, dipropylene glycol initiated, M_n = 2800 g/mol) were dried at 90 °C in a vacuum oven for 6 h before use.

2.2. Modification of VMT. The jet-milled VMT was modified with CTAB to create CTAB-VMT according to a method published previously.[21] Twenty grams of dried and jet-milled pristine VMT (P-VMT) powder was dispersed in 100 mL of 4 M sodium chloride solution and refluxed for 48 h. Interlayer metal cations, mainly hydrated Mg^{2+}, were exchanged with Na^+ by reflux with sodium chloride. The Na^+ exchanged VMT (Na-VMT) was centrifuged and separated, and then washed with deionized water and ethanol several times to remove Cl^-, then dried overnight in a vacuum oven at 90 °C. CTAB-VMT was synthesized by replacement of Na-VMT with the CTAB aqueous solution (120% excess CTAB of the measured effective cation exchange capacity of Na-VMT, 99 mequiv/100g) at 80 °C for 48 h. The CTAB solution treatment was repeated once, and then the product was separated by centrifugation. The final CTAB-VMT was washed several times with warm water after warm ethanol and dried overnight at 90 °C in a vacuum oven before use.

2.3. MDI and CTAB-VMT Dispersion. A polyol and clay preblend or **master-batch** (MB) was prepared with EO tipped Jeffol PPG-2801 (which is notated as EPO1400 in Table 1), dried CTAB-VMT, and toluene. EO-tipped and PO-central polyols have been clearly identified as effective intercalators for clay platelets in a PU matrix.[5] Different

Table 1. Formulation of the PU Rigid Films[a]

notation	trade name[b]	molecular weight	parts by weight
PO200	Jeffol G30-650 (25%)	260 g/mol	86
	Jeffol FX31-240 (75%)	700 g/mol	
EPO1400	Jeffol PPG-2801	2800 g/mol	20
MDI	Rubinate M	365 g/mol	80
Defoamer	BYK-88		0.06

[a]The formulation here is for the neat PU. Formulations of PU nanocomposites with CTAB-VMT are listed in the Supporting Information, Table S1. [b]Jeffol and Rubinate are registered trademarks of Huntsman Corporation or an affiliate thereof in one or more, but not all countries. BYK is a registered trademark of BYK-Chemie.

amounts of CTAB-VMT were added to the EPO1400 and toluene in capped 20 mL glass bottles and vigorously shaken. The mixtures were stirred with a magnetic stirrer for 30 min and then subjected to probe ultrasonication using a 2 mm diameter tapered micro tip (UP200S ultrasonic processor, Hielscher, 28% amplitude, 1 s cycle, 0.5 s sonication/0.5 s rest) for 30 min (3 cycles of 10 min sonication and 5 min pause) while being magnetically stirred. The MB was further dried under vacuum at 90 °C for 6 h which evaporated the toluene and removed moisture. The MB was denoted as MB_x, where x is the CTAB-VMT weight percentage in MB after toluene removal. The dried MB was dispersed in MDI and mixed using a high shear air-driven Cowles mixer (V322 High Speed Air Drill, Viking Air Tools) at 20,000 rpm for 5 min. This mixture was degassed under vacuum for 30 min and then magnetically stirred for at least 6 h. The resulting blends were denoted as MDI_MB_y, where y is the clay weight percentage in the dispersion.

For comparison, CTAB-VMT was directly added to MDI by the same ultrasonication and high shear mixing procedure but without EPO1400. We refer to this process as **direct mixing** in contrast to the **master-batch** method described above. We denote the resulting blends as MDI_CTAB-VMT_y.

2.4. Synthesis of PU Rigid Nanocomposites. Fabrication of void-free PU rigid films is critical for gas permeation tests. The formulation found in Table 1 was used to prepare these films. Voids were eliminated by minimizing exposure to air and moisture during PU synthesis and including addition of a defoamer in the formulation. PO200 polyol (1:3 by weight mixture of Jeffol G30-650:Jeffol FX31-240) was dried under vacuum and magnetically stirred at 90 °C for at least 6 h before use. The isocyanate index (the amount of isocyanate relative to the theoretical stoichiometric equivalent amount in percentage terms, i.e., 1 mol NCO:1 mol OH = 100), of this formulation was maintained at 110 regardless of the CTAB-VMT content. The defoamer (BYK-88) was added to the PO200 and MDI_MB, which was then mixed at 20,000 rpm for 5 min followed by 30 min vacuum degassing. The final blend was poured on a high-density polyethylene (HDPE) plate and covered with another HDPE plate to minimize exposure to moisture and to control the film thickness. The polymer was cured at room temperature for 48 h and then at 95 °C in a vacuum oven for 24 h to ensure complete reaction. The resulting nanocomposites were denoted as PU_MB_z and PU_CTAB-VMT_z, indicating PU nanocomposites from MDI_MB and MDI_CTAB-VMT (direct mixing), respectively, where z is the CTAB-VMT wt % in the final composite. The notation for each sample used in this study is listed in Table 2. As an example, the MB_10 master-batch was dispersed in MDI (MDI_MB_2.0), which was then mixed with polyol to make the final composite, PU_MB_1.1.

2.5. Characterization. X-ray diffraction (XRD) patterns of VMT were obtained by using a PANalytical X-Pert Pro MPD X-ray diffractometer equipped with a Co source (45 kV, 40 mA, λ = 1.790 Å) and an X-Celerator detector. Small-angle X-ray scattering (SAXS) patterns of the MDI dispersions and PU nanocomposites were obtained from a Rigaku RU-200BVH 2D SAXS instrument with a Cu source (45 kV, 40 mA, λ = 1.542 Å) and a Siemens Hi-Star multiwire area detector.

Table 2. Notation for Each Sample Used in This Study

	master-batch	MDI dispersion	PU rigid film
MB mixing	MB_0[a]	MDI_MB_0	PU_MB_0 (neat PU)
	MB_10	MDI_MB_2.0	PU_MB_1.1
	MB_20	MDI_MB_4.0	PU_MB_2.2
	MB_30	MDI_MB_6.0	PU_MB_3.3
	MB_40	MDI_MB_8.0	PU_MB_4.4
direct mixing		MDI_CTAB-VMT_0[a]	PU_CTAB-VMT_0 (neat PU)
		MDI_CTAB-VMT_3.0	PU_CTAB-VMT_1.42
	N/A	MDI_CTAB-VMT_4.0	PU_CTAB-VMT_1.9
		MDI_CTAB-VMT_6.0	PU_CTAB-VMT_2.85
		MDI_CTAB-VMT_8.0	PU_CTAB-VMT_3.9

[a]MB_0 and MDI_CTAB-VMT_0 indicate the pure EPO1400 and pure MDI, respectively.

Rheological characteristics of the MDI_MB blends were measured using a TA Instruments AR-G2 stress-controlled rotational rheometer with a 40 mm cone plate at room temperature. Viscosity profiles were obtained under steady state flow as the shear rate was increased in logarithmic increments from 0.01 to 1000 s^{-1}.

Dispersion, intercalation, and exfoliation of CTAB-VMT were visualized with optical microscopy and TEM. The clay dispersion in the MDI_MB blend was evaluated by the optical microscope system (BH2-UMA, Olympus), and TEM images of final PU films were obtained on a FEI Tecnai T12 microscope using an accelerating voltage of 120 kV. Seventy nanometer thin sections of rigid films were obtained by microtoming solid PU samples at room temperature with a diamond knife and then transferred on 400-mesh Ni grids (Leica Ultracut).

Differential scanning calorimetry (DSC) measurements of the PU samples were carried out with a TA Instruments DSC Q1000. Five milligrams of sample was loaded into an aluminum standard pan, and scanning was performed from −100 to 200 °C at the rate of 10 °C/min after removing the thermal history with heating at 200 °C. The determination of the glass transition temperature was based on the inflection point method using TA Universal Analysis software.

Tensile moduli of neat PU and PU nanocomposite samples were measured using a Rheometrics Solid Analyzer-II. The samples were cut to 3 mm wide and 4 cm long rectangular thin film strips with 200 μm thickness and loaded on the film fixtures. After applying a pretension of 7 g force, a dynamic strain sweep at 1 rad/s from 0.001% to 1% strain was applied at room temperature, and the temperature dependence of the modulus was determined by a temperature ramp from −50 to 150 °C at 5 °C/min.

CO_2 gas permeation measurements of CTAB-VMT reinforced PU membranes with 80 to 100 μm thickness were performed with a homemade permeation cell at 25 °C.[22] The CO_2 permeability coefficient across the films was determined from the pressure change monitored as a function of time across the film, starting from initial pressures of 40−45 psi on one side of the film and ambient pressure on the other. Permeation constants were calculated by normalizing the pressure change by sample area and thickness, and the pressure difference across the film.[23]

3. RESULTS AND DISCUSSION

3.1. Modification of VMT. P-VMT is a layered, hydrated, magnesium aluminum iron silicate. The multivalent metal cations, such as Mg^{2+}, Al^{3+}, $Fe^{2+/3+}$, between P-VMT layers were exchanged to monovalent Na^{+}. XRD patterns were used to investigate the intercalation of VMT interlayers through organic modification by CTAB, as shown in Figure 2. An

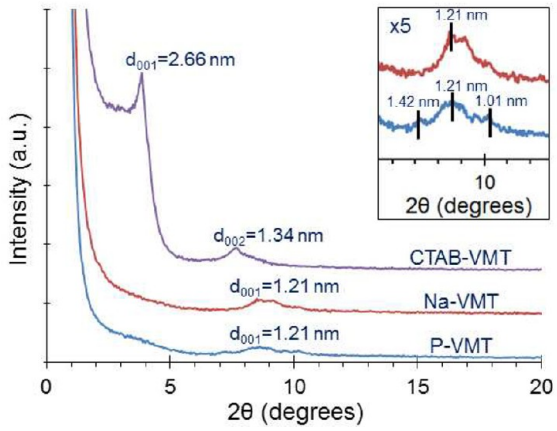

Figure 2. XRD patterns of VMT samples before and after modification: P-VMT, Na-VMT, and CTAB-VMT, vertically offset for comparison. The inset shows the five time enlargements of P-VMT and Na-VMT peaks. The intensities of the P-VMT and Na-VMT peaks are relatively low, because the same narrow slit was used for all the clay samples to enable low-angle characterization. The intensity of CTAB-VMT was high enough to also exhibit the secondary *d*-spacing (d_{002}).

increase in the interlayer spacing denoted as the *d*-spacing (d_{001}) can be monitored from P-VMT to CTAB-VMT. P-VMT had a major broad peak at 1.21 nm and other two minor peaks at 1.01 and 1.42 nm, indicating a mixture of different minerals and/or impurities.[24] Na-VMT shows the same major peak at 1.21 nm, while CTAB-VMT exhibits a larger d_{001}-spacing of 2.66 nm, because of formation of a paraffin complex in the intragallery space.[19]

3.2. VMT Dispersion in MDI. Intercalation of CTAB-VMT particles in the master-batch (MB) as well as in the sample directly mixed into MDI were monitored by SAXS. Figure 3

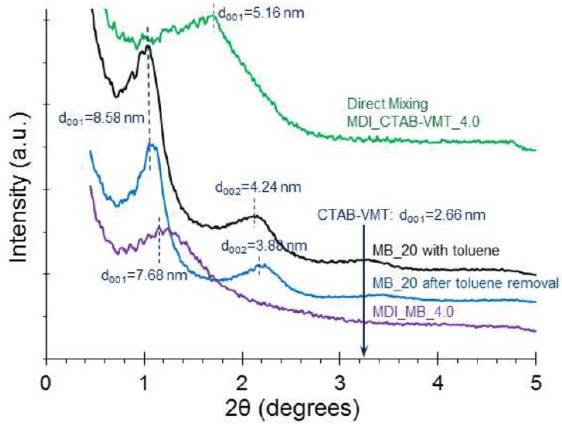

Figure 3. SAXS patterns of the master-batch before and after toluene evaporation and MDI dispersion with the master-batch. The direct mixture of MDI and CTAB-VMT is plotted for comparison.

shows the SAXS patterns of MB_20 (i.e., EPO1400 dispersion with 20 wt % CTAB-VMT), MDI_MB_4.0 (i.e., MDI and EPO1400 mixture with 4 wt % CTAB-VMT), and MDI_CTAB-VMT_4.0 prepared via direct mixing without EPO1400. CTAB-VMT swells to 8.58 nm in MB from 2.66 nm of dried CTAB-VMT because of intercalation of EPO1400 between clay layers. In previous studies, it has been reported that the EO tips aid penetration of this polyol into the

dx.doi.org/10.1021/am303244j | ACS Appl. Mater. Interfaces 2013, 5, 3054−3062

interlayer space.[5,25] The hydrophilic EO end groups strongly interact with the VMT surface, while the organophilic PO blocks interact with the organic modifier, CTAB. SAXS patterns did not show any sign of shrinkage after toluene removal, indicating that a major cause of intercalation is interaction with EPO1400, not with toluene. After MB_20 was dispersed in MDI (sample MDI_MB_4.0), the *d*-spacing decreased from 8.58 to 7.68. This shrinkage may be caused by changing the surrounding environment from EPO1400 to MDI. MDI molecules (M_n = 365 g/mol) are relatively smaller than EPO1400 (M_n = 2800 g/mol). The intensity of the d_{001} peak for MB_20 and MDI_MB_4.0 decreased because of a decrease in concentration of CTAB-VMT. MDI_MB_4.0 does not show the d_{002} because of insufficient clay concentration. Also, the broadening and reduction in intensity of the d_{001} peak in MDI_MB_4.0 showed that the layered structure did not have one distinct spacing, which suggests the random expansion and partial exfoliation of clay platelets.[5,6] The directly mixed sample, MDI_CTAB-VMT_4.0, shows a smaller *d*-spacing of 5.16 nm. MDI was not as effective in intercalation of CTAB-VMT as EPO1400.

Microscopic imaging is another tool to visually illustrate the state of nanofillers in a dispersing medium (see Supporting Information, Figure S2). The delaminated CTAB-VMT tactoids and some single layers in MDI dispersion are shown in the TEM microscopic images. This TEM observation agrees with the broad SAXS peak of the MDI dispersion, again indicating partial exfoliation of CTAB-VMT particles. The homogeneous distribution of CTAB-VMT particles throughout the medium is another key factor of a good MDI dispersion and uniform distribution of clay in the PU nanocomposite. Optical microimaging confirmed the good distribution and break-up of the CTAB-VMT agglomerates by high shear mixing.

3.3. Rheological Characterization of MDI Dispersion. Figure 4a shows the viscosity of MDI_P-VMT_3.0 and MDI_CTAB-VMT_3.0 via direct mixing as a function of shear stress. With CTAB-VMT, the dispersion showed strong shear thinning, whereas Newtonian behavior was observed for neat MDI and the dispersion with P-VMT. Shear thinning came from swelling of CTAB-VMT by the MDI and from a 3-dimensional network of clay platelets within the MDI matrix. On the other hand, MDI with 3 wt % P-VMT showed only a small increase in viscosity, indicating that the P-VMT was not exfoliated but remained in thick layered stacks.

The viscosity profiles of MDI dispersions with different concentrations of CTAB-VMT are shown in Figure 4b. All dispersions with CTAB-VMT exhibited a strong shear thinning effect, which is typical for colloidal dispersions with high-aspect-ratio particles, in contrast with the Newtonian flow behavior of the neat MDI. The viscosity of MDI_MB_2.0 increased significantly compared to neat MDI or MDI_MB_0 (i.e., MDI and EPO1400 mixture at a ratio of 80 to 20 by weight without CTAB-VMT). With 2 wt % of CTAB-VMT, the yield stress was 10 Pa, while for both mixtures with 4 and 6 wt % CTAB-VMT loading, the yield stresses were 50 and 500 Pa, respectively. The viscosity dramatically increased by increasing the content of CTAB-VMT and all dispersions showed strong shear thinning. Although this result indicates good dispersion of CTAB-VMT in MDI, high viscosity and high yield stress may interfere with the mixing needed to make PU composites. Mixing can only occur in regions where the stress exceeds the yield strength.

The formation of a gel-like structure in the MDI dispersions is further demonstrated in Figure 4c. Different from the pure

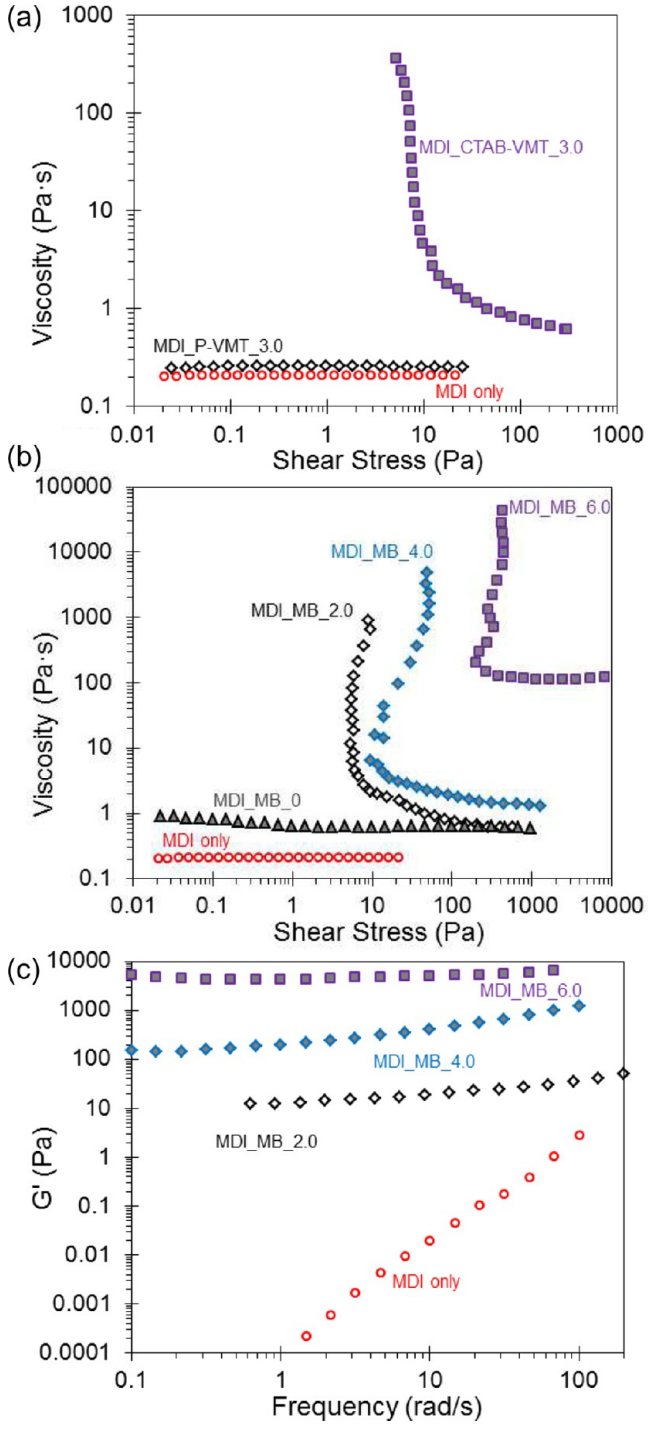

Figure 4. (a) Steady shear viscosity of MDI dispersions with 3 wt % P-VMT and CTAB-VMT by direct mixing. (b) Viscosity as a function of shear stress and (c) dynamic storage shear modulus profiles of neat MDI and MDI_MB dispersions with different concentrations of CTAB-VMT.

MDI, the storage modulus, G', is nearly independent of frequency, indicating the formation of a solid-like network, and it can be used to evaluate the strength of the network.

3.4. PU-VMT Rigid Nanocomposites. As mentioned in the rheological characterization section, high viscosity and high yield stress of MDI_MB dispersions at high CTAB-VMT concentration can result in insufficient mixing in MDI dispersion and imperfect dispersion of clay in the PU matrix.

dx.doi.org/10.1021/am303244j | ACS Appl. Mater. Interfaces 2013, 5, 3054−3062

MDI dispersions with 8 wt % CTAB-VMT and higher became highly viscous pastes (see Supporting Information, Figure S3). Note that the PU synthesis was only performed with up to MDI_CTAB-VMT_8.0 dispersion because of the difficulty of obtaining uniform films without clay aggregates and/or voids. The amounts of CTAB-VMT were 2, 4, 6, and 8 wt % in MDI_MB mixtures, which correspond to 1.1, 2.2, 3.3, and 4.4 wt % in PU rigid films, whereas MDI_CTAB-VMT_4.0 corresponds PU_CTAB-VMT_1.9 because of the absence of EPO1400 via direct mixing.

Figure 5 exhibits SAXS patterns that inform about the extent of CTAB-VMT dispersion in PU final nanocomposites.

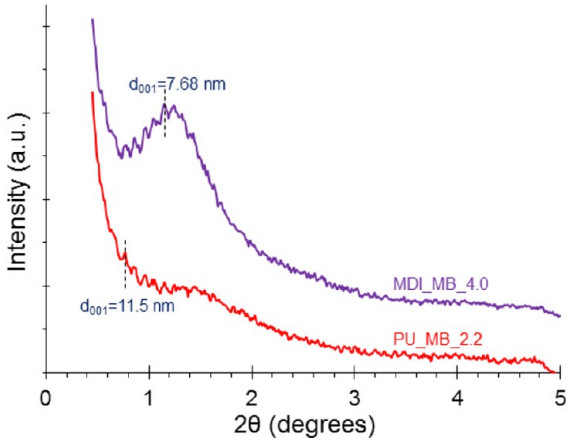

Figure 5. SAXS patterns of an MDI_MB_4.0 dispersion and a final PU_MB_2.2 film.

PU_MB_2.2 was produced by in situ polymerization of MDI_MB_4.0 and PO200. The scattering angle of 2θ = 0.77° indicates a d-spacing of 11.5 nm. Also, the extent of CTAB-VMT exfoliation in the final composites was characterized by X-ray scattering and TEM. The absence of X-ray peaks is often considered to be a good indication of exfoliation. The broad peak of PU_MB_2.2 indicates "exfoliation" of CTAB-VMT layers after high shear mixing and polymerization. This conclusion is supported by the TEM analysis results discussed below. Most CTAB-VMT particles in the PU nanocomposite were exfoliated, as shown in Figure 6. Thus, it would be reasonable to assume that a few stacked CTAB-VMT platelets were still left unexfoliated during PU polymerization, and contributed to a weak SAXS intensity at higher 2θ, ~ 1.5°.

TEM micrographs in Figure 6 illustrate a highly interdiffused nanostructure, in which the dark and light gray areas are CTAB-VMT-rich and PU-rich regions, respectively. In addition to highlighting the inner structure, the TEM images verify the size of individual CTAB-VMT particles and the change in the interlayer spacing. Nearly exfoliated and single sheets of CTAB-VMT are observed in the PU rigid nanocomposites produced from MB dispersion, PU_MB_2.2 and PU_MB_4.4. In agreement with the above X-ray scattering results, diffusion of EPO1400 to organoclay interlayers and high shear mixing promoted intercalation and exfoliation. This procedure (i.e., first, dispersing CTAB-VMT in EPO1400 and then MDI) also contributed to an even distribution of clay sheets throughout the PU matrix. Better dispersion of CTAB-VMT in PU may be attributed to distributive mixing as well as better intrinsic compatibility between CTAB-VMT and EPO1400 than MDI.

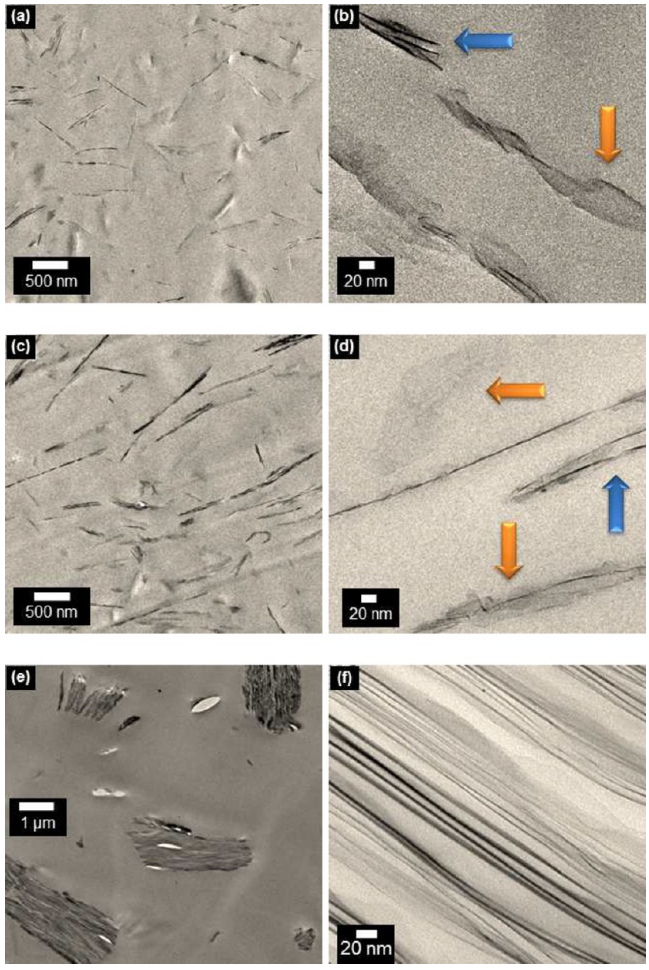

Figure 6. TEM images of (a, b) PU_MB_2.2, (c, d) PU_MB_4.4, and (e, f) PU_CTAB-VMT_1.9 rigid nanocomposites. The arrows in higher magnification images indicate fully exfoliated (yellow) and highly intercalated (blue) CTAB-VMT layers. Small cavities around and inside the tactoids in (e) are created during microtoming of the 70 nm thin sections containing the slices of rigid thick particles.

In contrast, TEM micrographs (e) and (f) show the inner structure of PU_CTAB-VMT_1.9 with stacks of clay platelets (or tactoids) and no observable exfoliation. Compared to PU_MB_2.2, very few exfoliated clay sheets are observed in the PU nanocomposites produced using direct mixing. Even with high shear mixing, the shear force was not enough to refine tactoid dimensions, though the large clay agglomerates broke, and smaller stacks (or tactoids) were distributed everywhere inside the PU matrix.

3.5. Mechanism of Clay Exfoliation in MDI-Clay Dispersion and PU Composites. Figure 7 suggests a possible mechanism of CTAB-VMT exfoliation in the MDI_MB dispersion and the PU nanocomposite. The mechanism can be summarized as follows. (1) Initially, VMT layers swell up after the interlayer ion exchange with CTAB, as explained previously and illustrated in Figure 7a. (2) During MB dispersion, it is found that the CTAB-VMT agglomerates break-up first, as a consequence of stirring and sonication in the presence of toluene. Simultaneously, EPO1400 penetrates into the layers of the organoclay. The presence of hydrophilic EO tips can help the EPO1400 to access the interlayer space and easily interact with the clay surface, while the less polar PO blocks interact with the organic modifier, CTAB. Increased

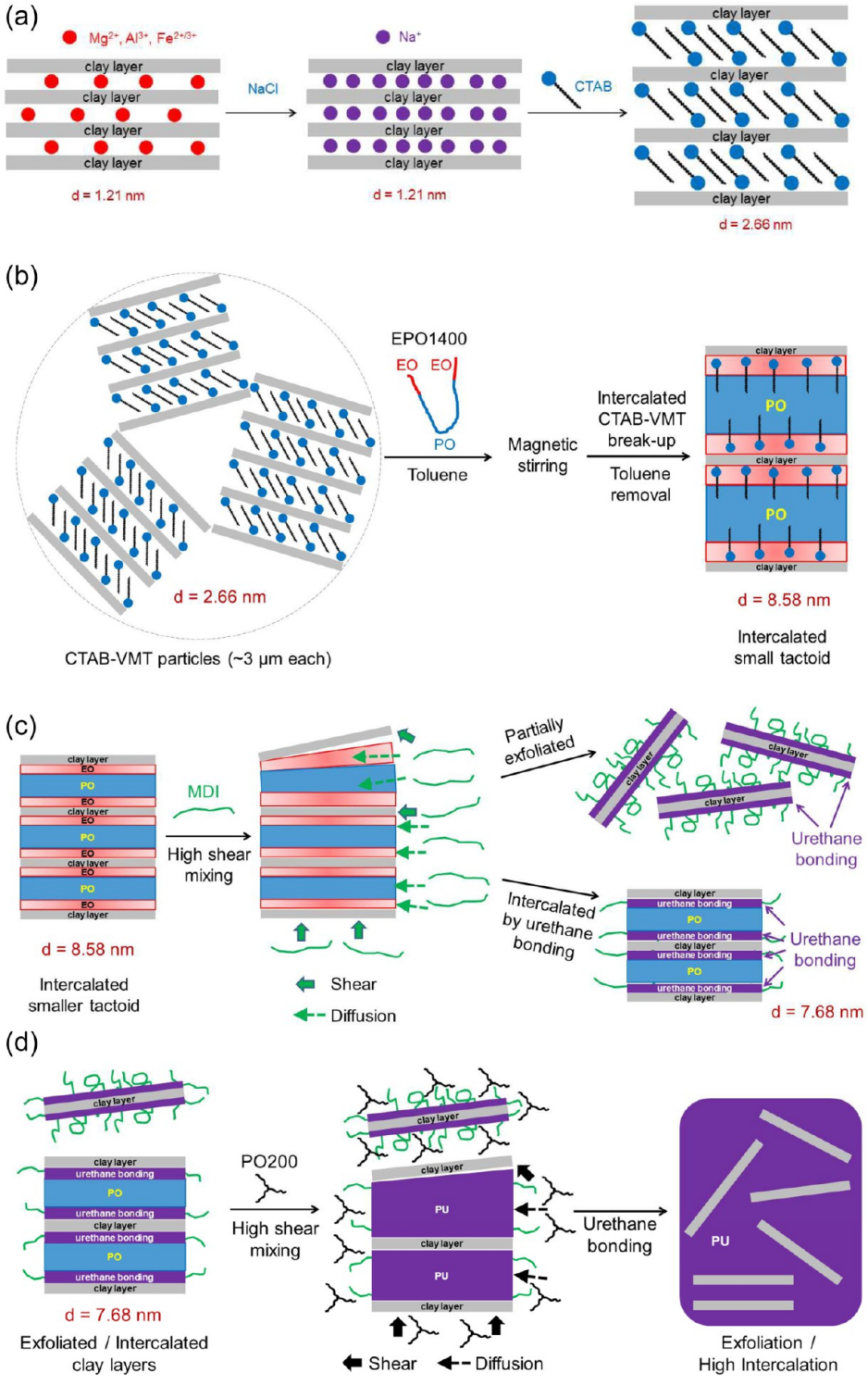

Figure 7. Stepwise mechanism of CTAB-VMT exfoliation in MDI_MB dispersion and PU nanocomposite: (a) layer expansion via organic modification, (b) clay particle break-up and intercalation through MB mixing and sonication, (c) partial exfoliation in MDI dispersion due to high shear mixing, and (d) platelet exfoliation and high intercalation in the PU nanocomposite.

intergallery elastic forces enhance the *d*-spacing because of interactions between CTAB-VMT and EPO1400. This intercalation process is depicted in Figure 7b. (3) Then, dispersed in MDI, intercalated tactoids break-up and partial platelet exfoliation occurs by high shear mixing, as shown in Figure 7c. Some platelets, especially those on the top or bottom of a stack, peel apart by combined diffusion and shear processes. Isocyanate end groups of MDI form urethane bonds with hydroxyl groups at the end of EO tips. The inner structure between clay layers is still polar after the urethane bonding. Simultaneously, polymeric MDI macromolecules penetrated between clay layers can maintain a high *d*-spacing. (4) Exfoliated or intercalated clay layers dispersed in MDI are mixed again with PO200. The relatively small PO200 molecules (MW = 600 g/mol) easily penetrate in, intercalate, and exfoliate the organoclay layers during high shear mixing.

dx.doi.org/10.1021/am303244j | ACS Appl. Mater. Interfaces 2013, 5, 3054−3062

Urethane bonds between remaining MDI and PO200 molecules form the PU matrix. Exfoliated VMT platelets and/or stacks of few clay layers (small tactoids) are dispersed in the PU matrix during high shear mixing and show very high aspect ratio. SAXS results are in good agreement with this mechanism.

The exfoliated VMT platelets can be found only in the case of MB mixing, as shown in TEM images of the final PU nanocomposites (Figure 6). The CTAB-VMT platelets with 3 nm thickness and ~1 μm length have very high aspect ratios, resulting in remarkable enhancements of mechanical and gas barrier properties. On the other hand, direct mixing without EPO1400 did not produce full exfoliation of CTAB-VMT platelets, but smaller tactoids due to shearing of platelet stacks were generated. It was confirmed on the TEM evidence that the *d*-spacing of CTAB-VMT, 2.66 nm, is not enough to exfoliate the clay layers by diffusion of MDI molecules. Larger clay tactoids are about 1 μm thick and 2−4 μm long in TEM micrographs, indicating that very little exfoliation or even break-up of CTAB-VMT particles had occurred.

3.6. Mechanical and Thermal Properties of PU Nanocomposites. Storage tensile moduli, E', and glass transition temperatures, T_g, of neat PU and PU nanocomposites are listed in Table 3. The addition of CTAB-VMT to PU induced a significant increase in E', as shown in Figure 8 by dynamic mechanical analysis (DMA) results (for further details, see Supporting Information, Figure S5). The increase in E' results from a high aspect ratio of CTAB-VMT platelets as a consequence of their uniform dispersion and high exfoliation, as shown in TEM micrographs. The tensile modulus of the PU nanocomposite at 25 °C was improved by 52% for PU_MB_2.2 from 0.98 to 1.49 GPa and 105% for PU_MB_4.4. At −20 °C there were also improvement in E' by 56% and 102% at PU_MB_2.2 and 4.4, respectively. Significant enhancement in mechanical properties of PU nanocomposites were shown at a temperature above T_g (72% and 178% at 120 °C, respectively) because of more effective hardening of the rigid nanofillers due to the lower neat PU modulus. It is also the reason that the low modulus elastomer exhibited a significant enhancement of tensile properties by the addition of clay. The improvement of the rigid composites in this study was not as much affected by the addition of clay as that of the elastomer composites. In the previous study, PU elastomer nanocomposites showed increases in E' of 128% and 177% at CTAB-VMT loadings of 1.4 wt % and 2.7 wt %, respectively.[5] Also, PU nanocomposites by MB dispersions exhibited more enhancement of E' than those by direct mixing without EPO1400 assistance. For PU_CTAB-VMT_1.9, the tensile modulus increased by only 27% over neat PU at 25 °C (see Supporting Information, Figure S6), because CTAB-VMT layers, which were well dispersed and exfoliated in PU via MB dispersion, had a much higher aspect ratio than those via the direct mixing procedure.

Table 3. Clay Volume Fraction, ϕ_{clay}, Glass Transition Temperatures, T_g, from DSC Analysis, tan δ Peak Temperatures, and Storage Tensile Moduli, E', from DMA, of neat PU and PU Nanocomposites

				E'		
sample	ϕ_{clay} (%)	T_g (°C)	tan δ peak (°C)	−20 °C (GPa)	25 °C (GPa)	120 °C (MPa)
Neat PU	0	66.6	73.3	1.36	0.98	10.5
PU_MB_1.1	0.39	67.7	72.5	1.57	1.19	15.0
PU_MB_2.2	0.79	69.2	76.5	2.12	1.49	18.1
PU_MB_3.3	1.19	70.7	77.6	2.57	1.81	22.3
PU_MB_4.4	1.60	74.4	76.7	2.75	2.01	29.2

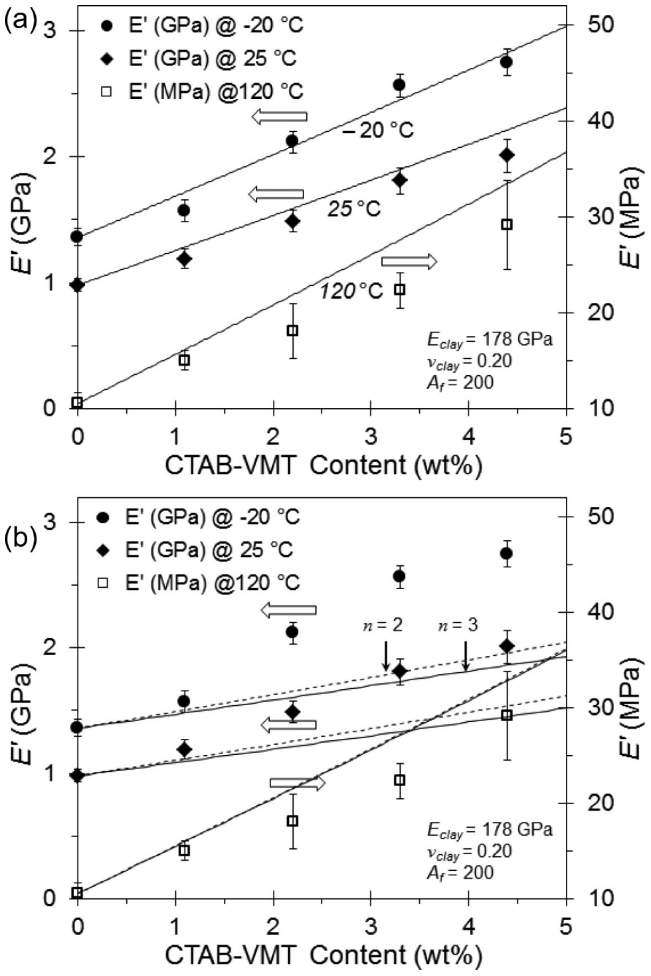

Figure 8. Experimental and theoretical modulus data for CTAB-VMT PU nanocomposites. (a) The Mori−Tanaka theoretical prediction assumes unidirectional alignment of clay of 178 GPa and A_f = 200 (a) with n = 1 (solid lines), and (b) n = 2 (dotted line) and 3 (solid line), respectively.

The Mori−Tanaka model modified by Tandon and Weng was used to predict the tensile modulus of composites with rigid fillers based on clay fraction and aspect ratio (A_f).[27,28] The aspect ratio of exfoliated clay sheets was estimated by using the analytical formula and material parameters (see Supporting Information). In the calculation, the effective clay particle is represented by a multilayer stack of VMT platelets and gallery material, as described previously (Supporting Information, Figure S7).[29,30] Figure 8 shows that the experimental data are in good agreement with the assumption of clay exfoliation with A_f of ~200, indicating that each clay platelet acts as the reinforcing filler particle (n = 1). It should be noted that the A_f of CTAB-VMT from Mori−Tanaka modeling, 200, appears to be smaller than A_f of exfoliated clay sheets estimated from TEM analysis (500−1000, Figure 6 and Supporting Information, Figure S2a). The smaller A_f from modulus calculation may be due to a combination of clay particle orientation, a distribution of layer stacks, and curved layers. The Mori−Tanaka model is based on

monodispersed ellipsoids with perfect planar orientation. However, the clay particles showed a partly random orientation, as seen in the TEM images. Second, although CTAB-VMT platelets are mainly dispersed as exfoliated sheets, some are intercalated tactoids of different thickness so that these stacks may diminish modulus and A_f compared with exfoliated sheets. Also, because of their flexibility, the curved or rolled clay layers may contribute less to reinforcement of modulus than theoretically predicted.

The glass transition temperatures, T_g, of neat PU or PU nanocomposites, determined by DSC, are also listed in Table 3. From DSC scans, the neat PU and the PU nanocomposites have very similar behavior of T_g around 67 to 75 °C, with an increase in T_g at higher CTAB-VMT concentrations. In the literature, both increases and decreases in T_g have been reported.[5,10,12,26,31,32] Although there may still be uncertainty of the change in T_g of the polymer with the addition of nanofillers, the T_g of the polymer is affected by its environment and the interaction between the matrix and the filler. The increase in T_g of nanocomposites is a result of the strong interactions between CTAB-VMT and PU and the confinement of PU molecules by nanodispersed CTAB-VMT platelets, indicative of restricted segmental mobility of the polymer chains. Similar to the T_g values measured by DSC, the peak temperatures in tan δ from DMA slightly increased with filler concentration. However, the increase is smaller, indicating that polymer chain relaxation is not highly sensitive to organoclay addition.

3.7. Gas Barrier Properties. An important goal of this study was to achieve significant enhancements in CO_2 gas barrier properties with a low loading of organoclay platelets. Sheet-like CTAB-VMT platelets can act as effective gas barrier components inside a polymer composite membrane reducing gas diffusion. CO_2 gas permeation, P_{CO2}, through PU nanocomposite films was tested at 25 °C using a water bath and plotted against the weight fraction of the clay particles compared to neat PU, as shown in Figure 9. PU_MB and PU_CTAB-VMT rigid films with different CTAB-VMT loadings were tested for comparison. A significant reduction in CO_2 gas permeation was observed for the films prepared by the master-batch procedure. The PU_MB_3.3 and 4.4 films could decrease P_{CO2} by ~40% compared to neat PU rigid films while a less significant reduction of ~20% could be achieved with the PU_CTAB-VMT_3.8 film prepared by direct mixing. This 30 or 40% reduction in P_{CO2} is much higher than 10% reduction achieved with a PU_P-VMT_5.0 film prepared by direct mixing.

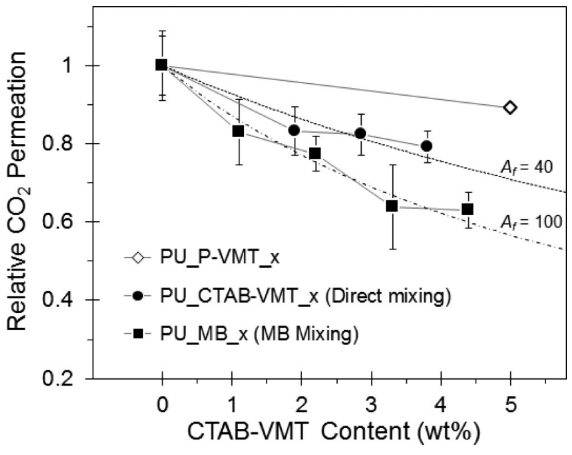

Figure 9. Relative CO_2 gas permeability of several nanocomposite films as a function of the weight fraction of VMT. The dotted curves are theoretical predictions based on Fredrickson and Bicerano at aspect ratios of 40 and 100, respectively.[33].

The relative P_{CO2} versus VMT fraction was fitted with a gas permeation model modified by Fredrickson and Bicerano.[33] This model assumes that nanoplatelets of the same aspect ratio are arranged randomly but parallel to each other and perpendicular to the diffusion direction (see Supporting Information). The 40% decrease in P_{CO2} of PU_MB is comparable with A_f = 100. It should be noted that this A_f value, 100, is smaller than the higher A_f of 500−1000 estimated from TEM analysis or the value of 200 from the modulus improvement. This significant decrease in aspect ratio is most likely coming from the misalignment of exfoliated clay layers. It is clear in Figure 6a and 6c that the clay platelets are not parallel to each other. In addition, the interface can be affected by surface properties of clay particles, and an incompatible surface chemistry may cause some defects in the interfaces, which can create voids, increase the free volume, and eventually lead to increased permeability.

4. CONCLUSIONS

VMT modified by quaternary ammonium cations was used to improve properties of a PU film, especially gas barrier performance and mechanical properties. These impermeable CTAB-modified VMT sheets may be used to reduce diffusion of the blowing agent (i.e., CO_2 gas) from the cell structure of rigid PU foams. CTAB-VMT dispersion in polymeric MDI can be improved with the aid of a polyol dispersion with EO tipped polyol (EPO1400). Significant shear-thinning effects (i.e., viscosity and linear viscoelasticity increase, and development of yield stress) were observed in MDI_MB mixtures, indicating good dispersion of CTAB-VMT in MDI. The large interlayer spacing of CTAB-VMT because of intercalation of EPO1400 resulted in better dispersion of CTAB-VMT in MDI, and thus this MDI_MB dispersion was used for synthesis of improved rigid PU nanocomposites.

PU nanocomposite films were prepared by mixing selected polyol blends (PO200) with MDI_MB master-batches. TEM micrographs indicated that CTAB-VMT sheets were highly intercalated and exfoliated. The polyol-assisted CTAB-VMT blending method caused significant improvements in intercalation and exfoliation, in contrast to the large thick CTAB-VMT particles in the matrix obtained by the direct mixing method without EPO1400 assistance. The organoclay dispersion also led to a significant increase in tensile stiffness. Compared to neat rigid PU, a 52% increase in storage modulus was observed with only 2 wt % loading of CTAB-VMT. With 3 wt % CTAB-VMT, CO_2 permeation through rigid PU nanocomposites could be reduced to 60% compared to neat PU. The better dispersion of clay platelets in the polymer matrix, combined with a higher aspect ratio due to exfoliation of organoclay sheets, offered greater reductions in CO_2 permeation.

In summary, rigid PU nanocomposite films with organoclay particles showed improved gas barrier and mechanical properties. Bulk film samples were used as preliminary specimen to select the suitable PU system because of difficulties in testing mechanical properties and gas permeation of the foam samples. This study lays the groundwork for future studies to fabricate PU-organoclay nanocomposite foams and evaluate their characteristics.

■ ASSOCIATED CONTENT

Supporting Information

Particle size of jet-milled VMT, microscopy of MDI and CTAB-VMT dispersions, images of MDI dispersions with CTAB-VMT, additional DMA and DSC data of PU nanocomposites, Mori−Tanaka model for nanocomposite tensile moduli, and theoretic predictions of gas permeation through PU and CTAB-VMT nanocomposites. This material is available free of charge via the Internet at http://pubs.acs.org.

■ AUTHOR INFORMATION

Corresponding Author

*Tel: +1 612 625 0092. Fax: +1 612 626 1686. E-mail: a-stein@umn.edu (A.S.), macosko@umn.edu (C.W.M).

Notes

The authors declare no competing financial interest.

■ ACKNOWLEDGMENTS

The authors thank Huntsman Polyurethanes for providing technical and financial support. The authors also thank Mr. Jason Zhang, Mr. Reese Weber, and Mr. Ping Hung Tse for assistance in sample fabrication and mechanical testing. The TEM acquisition at the University of Minnesota Characterization Facility was supported by the NSF through the NNIN program. Some work was carried out at the College of Science and Engineering Polymer Characterization Facility, University of Minnesota, which receives support from the NSF through the MRSEC program.

■ REFERENCES

(1) Woods, G. *The ICI Polyurethanes book*; 2nd ed.; ICI Polyurethanes and Wiley: New York, 1990.
(2) Randall, D.; Lee, S. *The Polyurethanes Book*; Wiley: New York, 2002.
(3) Tan, S. Q.; Abraham, T.; Ference, D.; Macosko, C. W. *Polymer* **2011**, *52*, 2840.
(4) Modesti, M.; Lorenzetti, A.; Dall'Acqua, C. *Polym. Eng. Sci.* **2005**, *45*, 260.
(5) Qian, Y.; Lindsay, C. I.; Macosko, C.; Stein, A. *ACS Appl. Mater. Interfaces* **2011**, *3*, 3709.
(6) Widya, T.; Macosko, C. W. *J. Macromol. Sci., Part B: Phys.* **2005**, *44*, 897.
(7) Wang, Z.; Pinnavaia, T. J. *Chem. Mater.* **1998**, *10*, 3769.
(8) Chavarria, F.; Paul, D. R. *Polymer* **2006**, *47*, 7760.
(9) Chen, T. K.; Tien, Y. I.; Wei, K. H. *Polymer* **2000**, *41*, 1345.
(10) Cao, X.; James Lee, L.; Widya, T.; Macosko, C. *Polymer* **2005**, *46*, 775.
(11) Harikrishnan, G.; Patro, T. U.; Khakhar, D. V. *Ind. Eng. Chem. Res.* **2006**, *45*, 7126.
(12) Kim, S. H.; Lee, M. C.; Kim, H. D.; Park, H. C.; Jeong, H. M.; Yoon, K. S.; Kim, B. K. *J. Appl. Polym. Sci.* **2010**, *117*, 1992.
(13) Harikrishnan, G.; Lindsay, C. I.; Arunagirinathan, M. A.; Macosko, C. W. *ACS Appl. Mater. Interfaces* **2009**, *1*, 1913.
(14) Benham, A. J.; Brown, T. J. *African Mineral Production 2001−05*; British Geological Survey, 2007.
(15) Brown, T. J. *China and South East Asia Mineral Production 2001−05*; British Geological Survey, 2007.
(16) Tjong, S. C.; Meng, Y. Z.; Hay, A. S. *Chem. Mater.* **2002**, *14*, 44.
(17) Patro, T. U.; Harikrishnan, G.; Misra, A.; Khakhar, D. V. *Polym. Eng. Sci.* **2008**, *48*, 1778.
(18) Mittal, V. *J. Compos. Mater.* **2008**, *42*, 2829.
(19) Slade, P. G.; Gates, W. P. *Appl. Clay Sci.* **2004**, *25*, 93.
(20) Qian, Y.; Liu, W.; Park, Y. T.; Lindsay, C. I.; Camargo, R.; Macosko, C. W.; Stein, A. *Polymer* **2012**, *53*, 5060.
(21) Osman, M. A. *J. Mater. Chem.* **2006**, *16*, 3007.
(22) Phillip, W. A.; Rzayev, J.; Hillmyer, M. A.; Cussler, E. L. *J. Membr. Sci.* **2006**, *286*, 144.
(23) Cussler, E. L. *Diffusion: Mass Transfer in Fluid Systems*, 3rd ed.; Cambridge University Press: New York, 2009.
(24) Muiambo, H. F.; Focke, W. W.; Atanasova, M.; der Westhuizen, I. v.; Tiedt, L. R. *Appl. Clay Sci.* **2010**, *50*, 51.
(25) Lu, Y.; Kong, S.-T.; Deiseroth, H.-J.; Mormann, W. *Macromol. Mater. Eng.* **2008**, *293*, 900.
(26) Chiu, H. T.; Wu, J. H. *J. Appl. Polym. Sci.* **2005**, *98*, 1206.
(27) Mori, T.; Tanaka, K. *Acta Metall.* **1973**, *21*, 571.
(28) Tandon, G. P.; Weng, G. J. *Polym. Compos.* **1984**, *5*, 327.
(29) Fornes, T. D.; Paul, D. R. *Polymer* **2003**, *44*, 4993.
(30) Sheng, N.; Boyce, M. C.; Parks, D. M.; Rutledge, G. C.; Abes, J. I.; Cohen, R. E. *Polymer* **2004**, *45*, 487.
(31) Paul, D. R.; Robeson, L. M. *Polymer* **2008**, *49*, 3187.
(32) Shi, X.; Gan, Z. *Eur. Polym. J.* **2007**, *43*, 4852.
(33) Fredrickson, G. H.; Bicerano, J. *J. Chem. Phys.* **1999**, *110*, 2181.